ORIGINAL RESEARCH

Biosynthesis of Silver Nanoparticles from *Melia azedarach*: Enhancement of Antibacterial, Wound Healing, Antidiabetic and Antioxidant Activities

Gandhimathi Chinnasamy
Smitha Chandrasekharan [ID]
Somika Bhatnagar [ID]

Plant Transformation and Tissue Culture, Temasek Life Sciences Laboratory, National University of Singapore, 117604, Singapore

Purpose: Global demand for novel, biocompatible, eco-friendly resources to fight diseases inspired this study. We investigated plants used in traditional medicine systems and utilized nanotechnology to synthesize, evaluate, and enhance potential applications in nanomedicine.

Methods: Aqueous leaf extract from *Melia azedarach* (MA) was utilized for bio-synthesis of silver nanoparticles (MA-AgNPs). Reaction conditions were optimized for high yield and colloidal stability was evaluated using UV-Vis spectroscopy. MA-AgNPs were characterized by scanning electron microscopy (SEM), energy-dispersive X-ray (EDX), transmission electron microscopy (TEM), X-ray diffraction (XRD), and Fourier transform infrared spectroscopy (FTIR). Standard methods were used to analyze the antibacterial, wound healing, antidiabetic, antioxidant, and cytotoxic activities.

Results: The formation of MA-AgNPs at room temperature was confirmed by stable brown colloidal solution with maximum absorbance at 420 nm (UV-Vis Spectroscopy). MA-AgNPs were spherical (SEM), uniformly dispersed, 14–20 nm in diameter (TEM), and crystalline in nature (XRD). Presence of elemental silver was confirmed by peak at 3 KeV (EDX). FTIR data revealed the presence of functional groups which indicate phyto-constituents (polyphenols, flavonoids, and terpenoids) may have acted as the reducing and capping agents. MA-AgNPs (1000 µg/mL) showed larger zone of inhibition than MA-extract in the disk diffusion assay for human pathogenic gram positive bacteria, *Bacillus cereus* (34 mm) and gram negative, *Escherichia coli* (37 mm), thus confirming their higher antibacterial activity. The cell scratch assay on human dermal fibroblast cells revealed potential wound healing activity. The MA-AgNPs (400 µg/mL) demonstrated high antidiabetic efficacy as measured by α-amylase (85.75%) and α-glucosidase (80.33%) inhibition assays and antioxidant activity as analyzed by DPPH (63.83%) and ABTS (63.61%) radical scavenging assays. Toxic effect of MA-AgNPs against human chang liver cells (CCL-13) as determined by MTS assay, optical microscopic and CMFDA dye methods was insignificant.

Conclusion: This sustainable, green synthesis of AgNPs is a competitive alternative to conventional methods and will play a significant role in biomedical applications of *Melia azedarach*.

Keywords: medicinal plants, phytochemicals, nanotechnology, green synthesis

Correspondence: Somika Bhatnagar
Plant Transformation and Tissue Culture, Temasek Life Sciences Laboratory, 1 Research Link, National University of Singapore, 117604, Singapore
Tel +65-68727630
Email somika@tll.org.sg

Introduction

There is global demand for biocompatible, eco-friendly, cost-effective, and consistent supply of natural resources to discover novel bioactive compounds which are inert, less toxic and more stable than currently popular synthetic chemicals to be easily delivered to the target site. Traditional systems of medicine such as

Ayurveda, Kampo, Unani and Chinese have been using plants for treatment of many ailments and this knowledge is being explored in modern medicine for discovery of new drugs.[1,2]

Nanoparticles (NPs) have emerged as compounds of great scientific interest due to their small size (1–100 nm) which imparts novel physical and chemical properties compared to their bulk counterparts or fine particles and thus possible new applications in healthcare, food and feed, environmental care, cosmetics, optoelectronics, chemical, and biotechnology industry.[3] NPs are synthesized from several metals like gold, nickel, selenium, iron, zinc, silver etc. Unique properties of NPs made from silver such as easy reduction of silver salts to form zero valent silver, chemical inertness, electrical conductivity, being a good catalyst, antimicrobial agent and a biosensor make silver nanoparticles (AgNPs) a good choice for a variety of applications.[4] Physical and chemical methods available for synthesis of NPs are often expensive, multi-step, complicated and require high voltage, high temperature, toxic solvents, and produce residues and hazardous by-products that have adverse effects in biological applications and on the environment.[5] Biological methods of synthesizing NPs utilize bacteria, fungi, algae, plant extracts, enzymes, proteins, polysaccharides or DNA.[5,6] This method does not require an external stabilizing agent as the phyto-constituents (such as terpenoids, flavonoids, polyphenols, saponins, tannins, amides, and carboxylic acids) themselves act as both reducing and capping agents, giving stability to the NPs.[7] This creates both a greener alternative and more variations in sizes and shapes of NPs, unlike chemical reducing agents where strong reagents result in larger size NPs while weak reagents slow down the process.[8] Additionally, coronas are formed on the surfaces of NPs as they slowly adsorb biomolecules; this leads to better interactions with the biological systems.[9] Use of plants is more advantageous than microorganisms, as plants can be easily grown outdoors on a large scale, while microbes require stringent, sterile lab and culture conditions for growth. Further, plant extracts are easy to use, inexpensive to produce, and offer a range of bioactive elements compared to just using individual biomolecules such as DNA, peptide, enzyme or protein (which are also prone to contamination and degradation).[5] In recent times, synthesis of AgNPs from plants has advanced dramatically, focusing on improving diagnosis, treatment, drug development, and targeted drug delivery systems and has huge potential for treatment of diseases such as cardiovascular, cancer, HIV/ AIDS, fungal and bacterial infections.[10–13]

For our studies we chose *Melia azedarach* (MA), a fast growing tropical tree which requires very minimal care and is mostly disease and pest resistant. It is cultivated in Australia, China, India, South America, and South-East Asia. In plantations, the bole is commonly utilized as fuelwood and plywood while the rest of the plant parts get discarded as waste material. However, traditional medicinal systems have documented the use of leaves and fruits for antimalarial, anthelmintic, rheumatoid, antipyretic and blood detoxifying properties by tribes.[14] Scientists have explored the potential of nanoparticles synthesized from seeds in control of mosquito larvae, from bark in inhibiting food pathogens and from leaves as a protective vegetable coating and in inhibiting cancer cell lines.[15–19]

The current study was undertaken for green synthesizing AgNPs for multiple biomedical applications. Since MA is perennial, fast growing, and leaves are easily available in bulk as leftovers from plantations, we utilized the leaves for synthesis of nanoparticles. Employing non-toxic and biocompatible method of extraction with water as the solvent and bioactive compounds as reducing, capping, and stabilizing agents, the MA-AgNPs were synthesized at room temperature (RT, 25°C). Critical parameters such as concentration and ratio of reactants, pH and incubation time for the reaction were optimized. MA-AgNPs were characterized by standard techniques of UV-Vis spectroscopy, SEM, EDX, TEM, XRD, and FTIR and evaluated for antibacterial, wound healing, antidiabetic, antioxidant potential and cytotoxic effect. MA-AgNPs were found to be stable in colloidal solutions at RT and demonstrated enhanced biological activities in comparison with the crude extract.

Materials and Methods
Materials
Leaves of MA were collected from Temasek Life Sciences Laboratory premises, Singapore. Deionized water was used throughout the experiment. All the chemicals purchased were of commercial reagent grade from Sigma-Aldrich, Singapore. The *Bacillus cereus* ATCC 14579, *Escherichia coli* ATCC 25922, human dermal fibroblast cells ATCC PCS-201-012, and human chang liver cells ATCC CCL-13 were purchased from American Type Culture Collection (Rockville, MD, United States).

Preparation of Extract

Freshly collected leaves of MA were rinsed under running tap water. Clean leaves were shade dried for 10 days and blended into a coarse powder. Aqueous extract was prepared by addition of 10 g of leaf powder to 100 mL of water and the solution was incubated at 50°C in water bath for 30 min. The extract was cooled to RT, filtered through filter paper (Whatman No.1), and filtrate was stored as MA-extract at 4°C for further studies.

Preliminary Phytochemical Screening

MA-extract (1 mL) was subjected to preliminary phytochemical screening. In all the tests, reaction volume was made up to 5 mL with deionized water. Ferric chloride test – addition of few drops of 5% ferric chloride to the MA-extract changed the color to dark green, this indicated the presence of phenolic compounds. Salkowski test – 1 mL of chloroform and 1 mL of concentrated sulfuric acid were added to the MA-extract. Formation of red-brown color indicated the presence of terpenoids. Alkaline reagent test – addition of few drops of 1 M sodium hydroxide to MA-extract resulted in the formation of intense yellow color which changed to colorless by addition of few drops of dilute acetic acid, this indicated the presence of flavonoids.

Biosynthesis of MA-AgNPs
Synthesis

Synthesis of AgNPs was carried out by standard procedure[20] with slight modifications. Different parameters such as concentration of reactants, ratio of reactants, pH and incubation time were optimized by varying one reaction variable at a time while keeping the others constant. Different volumes of MA-extract (1 mL, 5 mL, and 10 mL) were aliquoted into separate Erlenmeyer flasks and silver nitrate (1 mM $AgNO_3$) was added to each. The reaction mixtures were incubated in the dark at 25°C. To optimize the strength of silver ion, different concentrations of $AgNO_3$ (0.5–2 mM) were added to a fixed amount (5 mL) of MA-extract. The pH range tested was from pH 4 to pH 11. In order to optimize incubation time, samples were drawn from the reaction mixture at regular time intervals (6 h) over a 24 h period. Centrifugation at 4500 rpm for 20 min resulted in collection of synthesized MA-AgNPs in the form of pellet which was washed thrice with water to remove traces of any unbound phyto-constituents. The air-dried pellet was stored at RT for further studies.

Colloidal Stability Test

The ability of inorganic silver nanoparticles to form stable colloids when it reacts with plant extract is referred to as the colloidal stability of green synthesized nanoparticles. Colloidal stability test was performed according to the standard protocol.[21] MA-AgNPs were added to five different solutions namely NaCl salt solution (1.8%, w/v), PBS buffer (pH 7.4), Dulbecco's Modified Eagle's Medium (DMEM), CM (complete culture medium) and deionized water. Absorbance was measured by UV-Spectrophotometer (UV1601, Shimadzu) between wavelengths ranging from 100–900 nm. Further, the on-shelf stability in deionized water was assessed at RT for up to 9 days. Absorbance was periodically measured by a UV-Spectrophotometer (UV1601, Shimadzu) between wavelengths ranging from 100–900 nm.

Characterization of Synthesized MA-AgNPs

Parameters involved in characterization of AgNPs provide a comprehensive view of the particle size, shape, arrangement, stability, and potential functional groups responsible for the bio reduction and nature of the synthesized nanoparticles. UV-Visible absorption spectra of the MA-AgNPs dispersed in water were recorded by spectrometer in the wavelength range 100–900 nm. Morphology of MA-AgNPs was determined by scanning electron microscopy (SEM, JEOL JEM-6360 OLV) using dried samples coated with gold (SCD 105 sputter coater). Energy-dispersive spectroscopy (EDX) was used to determine elemental composition of MA-AgNPs. Transmission electron microscopy (TEM) analysis was employed with JEOL JEM-1230 electron microscope operated at an accelerating voltage of 40 kV for examination of nanoparticle size and space distribution. TEM grids were prepared by placing a drop of sample in water dispersion on a carbon-coated copper grid and drying at RT. Structural properties of freeze-dried and powdered MA-AgNPs were investigated by X-ray diffraction (XRD) patterns with D8 X-ray diffractometer (Bruker Biosciences Corporation, Billerica, MA, USA) at a scan rate of 1 step/second. The samples were subjected to Cu-Kα radiation over an angular range of 20°-80° (2θ). The characteristic absorption spectra of MA-extract and MA-AgNPs were recorded in the frequency range of 4000–400 cm^{-1} using a Thermo Nicolet Nexus 670 Fourier transform infrared spectrometer (FTIR, Thermo Fischer Scientific. Waltham, MA, USA). The spectra were obtained by operating the same equipment in diffuse reflectance mode at 4 cm^{-1}.

Screening for Antibacterial Activity
Antibacterial Activity

Antibacterial activity against gram positive, *B. cereus* and gram negative, *E. coli* was tested separately by disk diffusion method of Kirby-Bauer.[22] Bacterial experiments were carried out in Muller-Hinton (MH) nutrient medium. Broth as well as agar plates were prepared. Cultures were grown overnight in MH broth on orbital shaker at 250 rpm and 28°C. Bacterial growth was measured as absorbance at 600 nm using a spectrophotometer (2100 pro UV-Vis, GE) against non-inoculated broth as control. Separate plates were prepared for the two strains; 20 μL of bacterial culture ($1x10^6$ CFU/mL) was spread evenly and plates were incubated overnight at 37°C. Thereafter, standard disks (6 mm diameter) were impregnated individually with 20 μL of water (negative control), Rifampicin (positive control), $AgNO_3$, MA-extract and MA-AgNPs at 1000 μg/mL. These disks were aseptically placed on the two bacterial plates and incubated for 24 h at 37°C. Diameter of zone of inhibition (ZOI) of bacterial growth was measured and taken as the marker for antibacterial activity.

Antibacterial Mechanistic Action

Antibacterial mechanistic action was studied by determining the change in the morphology of bacteria under SEM. In brief, 100 μL of bacterial cells at a concentration of $1x10^6$ CFU/mL were separately treated with 100 μL of water (negative control), $AgNO_3$, Rifampicin (positive control), MA-extract and MA-AgNPs (1000 μg/mL) for 6 h. The reaction mixture was centrifuged at $3000 \times g$ for 30 min. Phosphate buffered saline (PBS) was used for washing the pellet thrice before prefixing with glutaraldehyde (2.5%) for 30 min. This was followed by three more washes with PBS. Increasing concentration of ethanol (from 30% to 100%) over a period of 15 min each, facilitated the dehydration of the samples. Last step was addition of amyl acetate and drying by critical point drying method. SEM (at 10 kV accelerating voltage) was used to observe morphology of dried samples (after coating them in gold using an automatic sputter coater).

Evaluation of Wound Healing Potential

In vitro wound healing study was conducted according to the standard method[23] with slight modification. Human dermal fibroblast cells (HDFa) were cultured in complete medium of DMEM on a 6-well plate at a density of $5.0x10^5$ cells/well. The plates were incubated at 37°C in a humidified atmosphere containing 5% CO_2 for 24 h.

Cultured media were removed and the cells were washed thrice with PBS. Medium containing either water (negative control), $AgNO_3$, Rifampicin (positive control), MA-extract or MA-AgNPs at 1000 μg/mL concentration was used as the test samples. 1 mL of previously mentioned sample was added individually into a 6-well plate containing cells. The cells were scratched using sterile yellow tip and cell migration was observed under a Leica BM IRB microscope (10x magnification) after two time intervals (28 h and 48 h).

Evaluation of Antidiabetic Activity: α-Amylase and α-Glucosidase Enzyme Inhibition Assay

In vitro antidiabetic activity of $AgNO_3$, MA-extract and MA-AgNPs (concentrations 200 μg/mL and 400 μg/mL) was investigated by standard method[24] for α-amylase and α-glucosidase enzyme inhibition with slight modifications. Acarbose (200 μg/mL and 400 μg/mL) was used as the reference standard. Control was prepared without sample. For α-amylase assay – 500 μL of sample was aliquoted in a test tube and 500 μL of 0.2 mM phosphate buffer (pH 6.9) containing α-amylase solution (500 μg/mL) was added to it. This mixture was incubated for 10 min at RT followed by addition of 500 μL of 1% starch solution in 0.02 M sodium phosphate buffer (pH 6.9). Reaction was carried out for 10 min. Addition of 1000 μL of 3,5-Dinitrosalicylic acid (DNS) reagent stopped the reaction. The reaction mixture was incubated for 5 min in a boiling water bath before cooling down to RT. Addition of 10 mL water diluted the reaction mixture. Absorbance was measured at 540 nm using a microplate reader (infinite M200 Tecan). For α-glucosidase assay – 20 μL of each sample was added into a 96-well plate followed by addition of 200 μL of master reaction mixture {α-nitro phenyl β-D-glucopyranoside (NPG) and α-glucosidase assay buffer in the ratio 1:25}. This mixture was incubated for 20 min at RT. Absorbance (A) was measured at 405 nm. Enzyme activity inhibition was calculated as per the equation:

$$\% \text{ Inhibition} = (A_{Control} - A_{Sample}) / A_{Control} \times 100$$

Evaluation of Antioxidant Activity: DPPH and ABTS Assay

In vitro antioxidant activity of $AgNO_3$, MA-extract and MA-AgNPs (concentration 100–500 μg/mL) was investigated by 2,2-diphenyl-1-picrylhydrazyl (DPPH) and 2,2′-Azino-bis

(3-ethylbenzothiazoline-6-sulfonic acid) (ABTS) radical scavenging assays. DPPH assay was conducted according to standard protocol[25] with slight modifications. In brief, 100 μL of 0.1 mM DPPH was added to 100 μL of different concentrations of $AgNO_3$, MA-extract and MA-AgNPs and the mixture was incubated at RT for 30 min in the dark. Absorbance value of the decolorized solution was taken at 517 nm. The free radical scavenging activity against ABTS radical was evaluated by standard procedure[26] with slight modifications. In brief, 10 mL of 7.4 mM ABTS was mixed with 10 mL of 2.45 mM ammonium persulfate and the mixture was kept at RT for 16 h in the dark.100 μL of ABTS was added to 100 μL of sample and solution was incubated at RT for 20 min in the dark. Absorbance (A) value was taken at 734 nm. In both these experiments, butylated hydroxytoluene (BHT) was used as the reference standard. Control was prepared without sample. Percentage inhibition was calculated using the following equation:

$$\% \text{ Inhibition} = (A_{Control} - A_{Sample}) / A_{Control} \times 100$$

Screening for Cytotoxicity

MTS assay was performed according to standard protocol[27] with slight modifications to determine the cytotoxic effect of MA-AgNPs on human chang liver cells (CCL-13). DMEM supplemented with fetal bovine serum (10%) and penicillin (1%) was used to culture CCL-13 cells. The cultures were grown at 37°C in a humidified atmosphere containing 5% CO_2 until 80% cell confluence. Addition of trypsin EDTA detached the confluences of cells. Trypan blue was used to calculate the separated cells with the help of a hemocytometer. Effect of MA-extract and MA-AgNPs (1000 μg/mL) on growth of CCL-13 cells was observed at a plating density of 1×10^6 cells/mL. The incubation of cultures was carried out at 37°C in a humidified atmosphere containing 5% CO_2 up to 72 h. Samples were added to a 96-well plate followed by the addition of 20 μL of MTS reagent (1:5 ratios of MTS in serum free media) in each well and kept for 3 h at 37°C in a humidified atmosphere containing 5% CO_2. Microplate reader (infinite M200 Tecan) was used to measure the optical density of the product at 490 nm against untreated cells as the control. Further, the cell morphology was observed under optical microscope after 72 h of treatment with MA-extract and MA-AgNPs. In addition, 5-chloromethylfluorescein diacetate (CMFDA) fluorescent dye was used to detect the live cell image at 72 h.

Statistical Analysis

All the experiments were repeated thrice. The mean±standard deviation (mean±SD) was analyzed by Student's *t*-test for the calculation of significance level. Values were considered statistically significant at p≤ 0.01.

Results
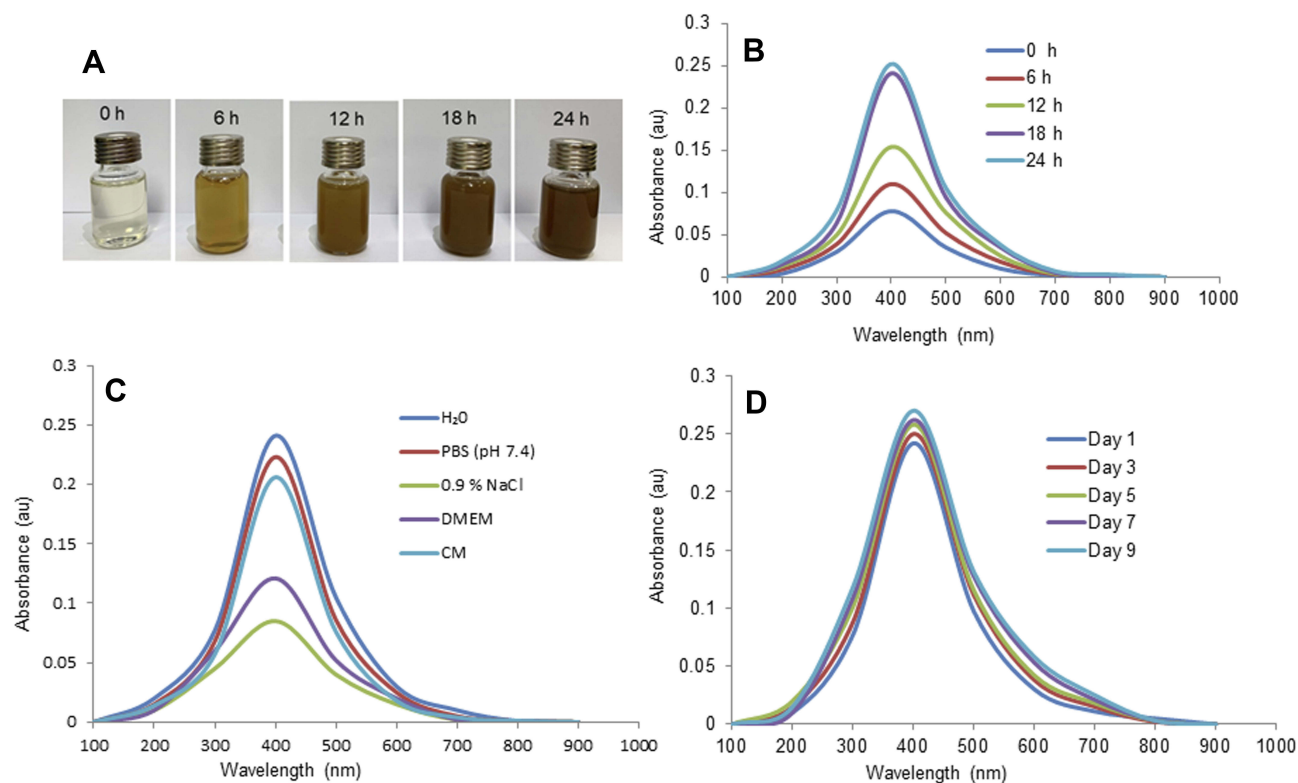## Biosynthesis of MA-AgNPs
Synthesis

Co-precipitation of MA leaf extract with $AgNO_3$ solution resulted in an immediate color change in the reaction mixture indicating the initiation of MA-AgNPs formation. With incubation, the color of the reaction mixture progressed from golden yellow to greyish brown finally stabilizing to a dark brown solution (Figure 1A). Surface plasma resonance peak at 420 nm further confirmed the formation of MA-AgNPs (Figure 1B). In the first experiment to find the optimal concentration of reagent and reactant necessary for synthesis of MA-AgNPs, maximum absorption in UV-Vis scanning was obtained when 45 mL of $AgNO_3$ was reacted with 5 mL of MA-extract and incubated overnight at RT. In the next experiment, different concentrations of $AgNO_3$ (ranging from 0.5–2 mM) were added to 5 mL MA-extract. The yield of MA-AgNPs increased with an increase in concentration of $AgNO_3$ up to 1 mM. Higher concentrations of $AgNO_3$ resulted in decreased yield of MA-AgNPs. 1 mM $AgNO_3$ was used in further studies. In addition to the concentration of the reagent and reactant ($AgNO_3$ and MA-extract), pH value of the reaction mixture is also a key factor for synthesis of MA-AgNPs. The yield of nanoparticle was found to be low at pH 6 and below. Sustainable increase in formation of nanoparticles with smaller diameter was seen at pH 7. Clusters of MA-AgNPs were observed at pH 10 and above. Thus, pH 7 was found to be optimum for maximum yield of MA-AgNPs. As the incubation period increased, MA-AgNPs continued to be formed, reaching the highest yield at 18 h; thereafter, the yield decreased due to insufficient reactants. In summary, the optimized parameters were – 5 mL of MA-extract, 45 mL of 1 mM $AgNO_3$, pH 7 with 18 h incubation at 25°C and 200 rpm in the dark.

Colloidal Stability

The synthesized MA-AgNPs were found to be highly stable in deionized water, PBS and CM (Figure 1C). The colloidal stability in deionized water was further plotted as absorbance in the given plot on different days. The

Figure 1 Green synthesis of MA-AgNPs. (**A**) Gradual color transition of MA-extract during synthesis of MA-AgNPs between 0 h and 24 h. (**B**) Corresponding UV-Vis spectra of synthesized MA-AgNPs. (**C**) Colloidal stability of MA-AgNPs under five different solutions: deionized water, phosphate buffered saline (PBS) (pH 7.4), NaCl (0.9%), Dulbecco's modified Eagle's medium (DMEM) and complete medium (CM). (**D**) On-shelf colloidal stability of MA-AgNPs at room temperature.

maximum absorbance peak was observed at 420 nm on all the days. This confirms that the MA-AgNPs were stable at RT for full test duration of 9 days (Figure 1D).

Characterization of Synthesized MA-AgNPs

SEM was used for the morphological characterization of MA-AgNPs. Mostly spherical and a few cuboidal MA-AgNPs were observed (Figure 2A). EDX analysis showed a strong signal in the silver region at 3 KeV, thus indicating development of MA-AgNPs (Figure 2B). Additional spectral signals were observed for oxygen (O), carbon (C), aluminum (Al), chlorine (Cl) and silicon (Si). Structural characterization carried out using TEM micrographic image (Figure 2) showed MA-AgNPs as spherical in shape and approximately 14–20 nm in size. The particles showed a mean size of 17.75±1.26 (Figure 2D). FTIR spectroscopy determined the absorption and transmission peaks which relate to the frequencies of vibrations between the bonds of the particles making up the material. Distinct peaks were observed at 1050 cm^{-1}, 1250 cm^{-1}, 1450 cm^{-1}, 1650 cm^{-1}, 2910 cm^{-1} and 3260 cm^{-1} in the MA-extract (Figure 2E). IR band at 1050 cm^{-1} indicates the C=O stretch of the alcoholic groups. Band at 1250 cm^{-1} is due to the

vibration of C-O group of the hydroxyl flavonoids. The band at 1450 cm^{-1} relates to CH_3, CH_2 flavonoids and aromatic rings where the vibration is the bending vibration of C-H and stretching vibration of aromatic rings. The band at 1650 cm^{-1} indicates the C=O stretching vibration of carboxyl groups. 2910 cm^{-1} peak indicates the CH vibration of methoxy group and the band at 3260 cm^{-1} is characteristic of C=C stretching vibration of the OH groups. In Figure 2E, a comparison of the spectra of MA-extract with the spectra of MA-AgNPs depicted absence of peaks at 2910 cm^{-1}, 1450 cm^{-1} and 1050 cm^{-1} in the latter, which indicates that there were no CH vibration of methoxy group, flavonoids and C-O group of hydroxyl flavonoids in the MA-AgNPs spectra. Preliminary phytochemical analysis which had detected the presence of flavonoids, terpenoids and phenolic compounds in the MA-extract also supported the interpretation of our FTIR results. These biomolecules are suggested as possible reducing and capping agent that contributed to the reduction of the silver ion, prevented the particles from coming in contact with each other, prevented aggregation and led to stabilization. XRD spectrum (Figure 2F) represents the four characteristic diffraction peaks of silver with 2θ values at 38.54°, 44.08°, 64.20° and 77.90°
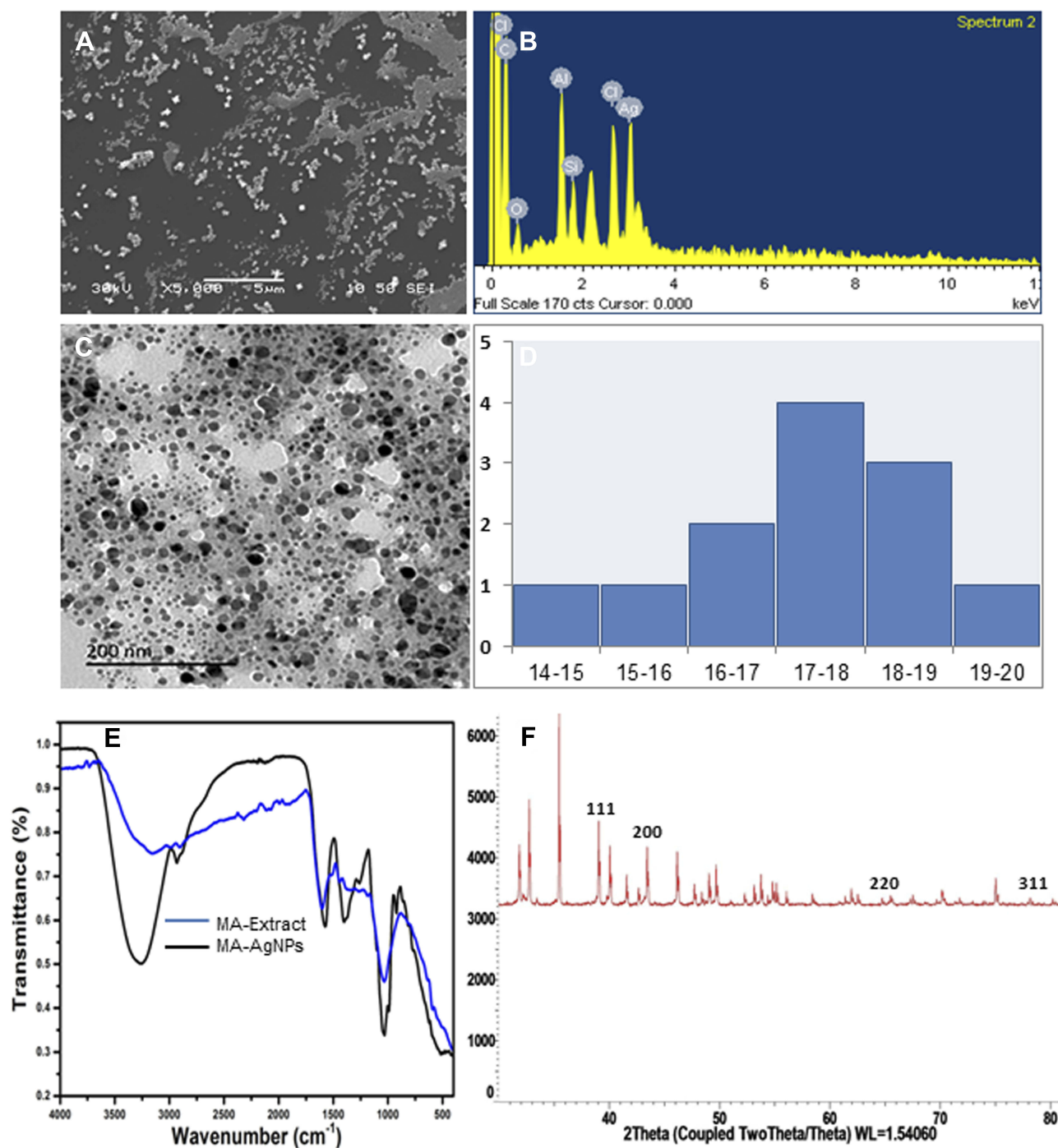
Figure 2 Characterization of green synthesized MA-AgNPs. **(A)** Surface morphology analysis under SEM. **(B)** Elemental analysis by EDX. **(C)** TEM image. **(D)** Particle diameter from TEM image. **(E)** FTIR spectra of MA-extract and MA-AgNPs. **(F)** XRD spectra.

corresponding to 111, 200, 220 and 311 lattice planes respectively.

Antibacterial Activity
Zone of Inhibition
ZOI was used as the criteria to determine the antibacterial effects of MA-extract and MA-AgNPs against *B. cereus*

and *E. coli*. The plates were monitored for bacterial growth at 12 h intervals (as shown in a representative Figure 3A). In both the bacterial cultures, no ZOI was observed in the untreated sample (a) and was negligible in AgNO₃ (b). MA-AgNPs (e) had a larger ZOI in comparison with MA-extract (d). Rifampicin (c) was used as positive control. The inhibitory effect increased up to 24 h
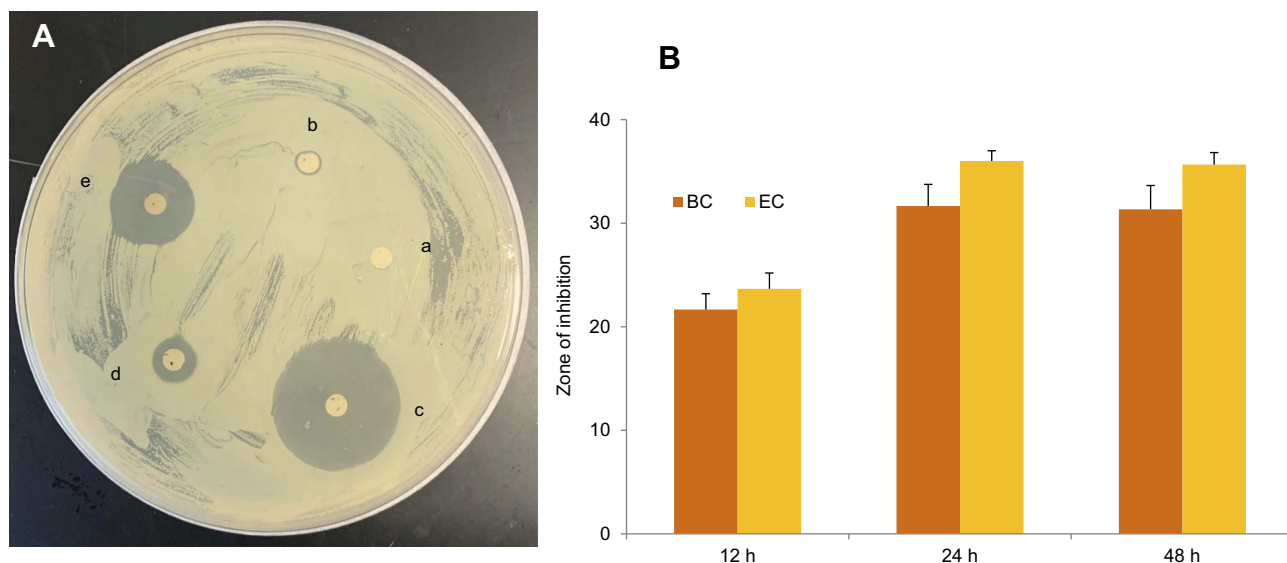
Figure 3 Antibacterial studies on *Bacillus cereus* and *Escherichia coli* by disc diffusion method. **(A)** Effect on growth of *E. coli* at 12 h of incubation: (a) negative control, (b) silver nitrate, (c) Rifampicin, (d) MA-extract, (e) MA-AgNPs. **(B)** Effect of MA-AgNPs on zone of inhibition (ZOI) of *Bacillus cereus* and *Escherichia coli* at different time intervals. **Abbreviations:** BC, *Bacillus cereus*; EC, *Escherichia coli*.
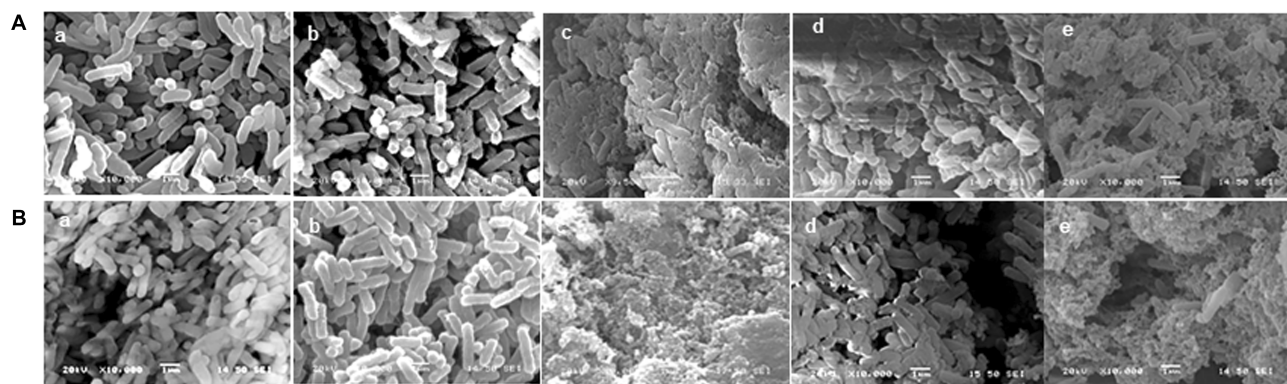
Figure 4 SEM image of antibacterial effect on **(A)** *Bacillus cereus* and **(B)** *Escherichia coli*: (a) negative control, (b) silver nitrate, (c) Rifampicin, (d) MA-extract, (e) MA-AgNPs.

with ZOI values for *B. cereus* and *E. coli* as $AgNO_3$ (8 mm, 10 mm), Rifampicin (33 mm, 38 mm), MA-extract (26 mm, 27 mm) and MA-AgNPs (34 mm, 37 mm) respectively. Thereafter, the ZOI for MA-AgNPs remained almost the same and no regrowth of bacteria was seen (Figure 3B). The result revealed that gram positive bacteria were less inhibited than gram negative bacteria.

Antibacterial efficacy was further tested by analyzing the cell viability of the formed bacterial colonies in the nutrient media. The colonies were picked from the margins of ZOI and cultured overnight in MH broth. Spectrophotometer analysis at 600 nm determined the viability of cells. As observed after 24 h, in the experiment with *B. cereus*, no growth was observed in MA-AgNPs. However, minimal growth was observed in MA-extract. The growth for *E. coli*

was minimal for MA-extract and MA-AgNPs. The bacterial cells showed significant growth in Rifampicin.

Antibacterial Mechanistic Action

The antibacterial mechanistic action was studied to determine the morphological changes. Due to smaller size, MA-AgNPs easily penetrated into the bacterial cell and exerted bactericidal effect as evident from SEM images (Figure 4A for *B. cereus* and Figure 4B for *E. coli*). Uniform cell texture was observed in untreated cells with an average size of 3 μm length and 1 μm width (a). The bacteria treated with $AgNO_3$ (b) showed least distortion while the treatment with Rifampicin had mostly ruptured cells (c). MA-extract had slightly distorted cellular structures (d) while the treatment with MA-AgNPs significantly damaged most of the bacterial cells (e).
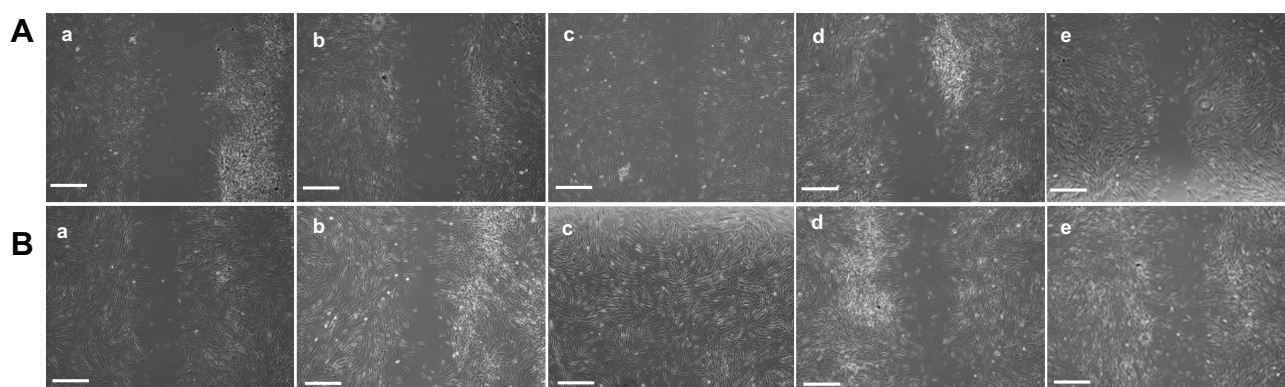
Figure 5 Wound healing effect on HDFa cells after **(A)** 24 h and **(B)** 48 h of treatment in (a) negative control, (b) silver nitrate, (c) Rifampicin, (d) MA-extract, (e) MA-AgNPs by the cell scratch assay at 10x magnifications (scale bar: 200 μm).

Wound Healing Activity

In vitro wound healing effect was determined by cell scratch assay on HDFa cell lines. Figure 5A shows that in comparison with the control (a) and AgNO₃ (b); Rifampicin (c), MA-extract (d) and MA-AgNPs (e) treated group had more cell migration on the wound site after 24 h. Furthermore, after 48 h a larger number of cells appeared in MA-AgNPs treated groups than the other groups (Figure 5B). The area of wound closure (%) was calculated as follows: 100 - (empty area at 48 h/empty area at 24 h)×100. Rifampicin (84%) had the highest

percentage of wound closure followed by MA-AgNPs (70.2%), MA-extract (62%), $AgNO_3$ (55%) and control (53%). This implies the wound healing potential of the MA-AgNPs.

Antidiabetic Activity

At the concentration of 200 μg/mL, MA-AgNPs displayed 82.43±1.92% α-amylase inhibition and at 400 μg/mL, inhibition was 85.75±1.20% (Figure 6A). The result confirmed that as compared to MA-extract, MA-AgNPs exhibited greater α-amylase inhibition activity. With the
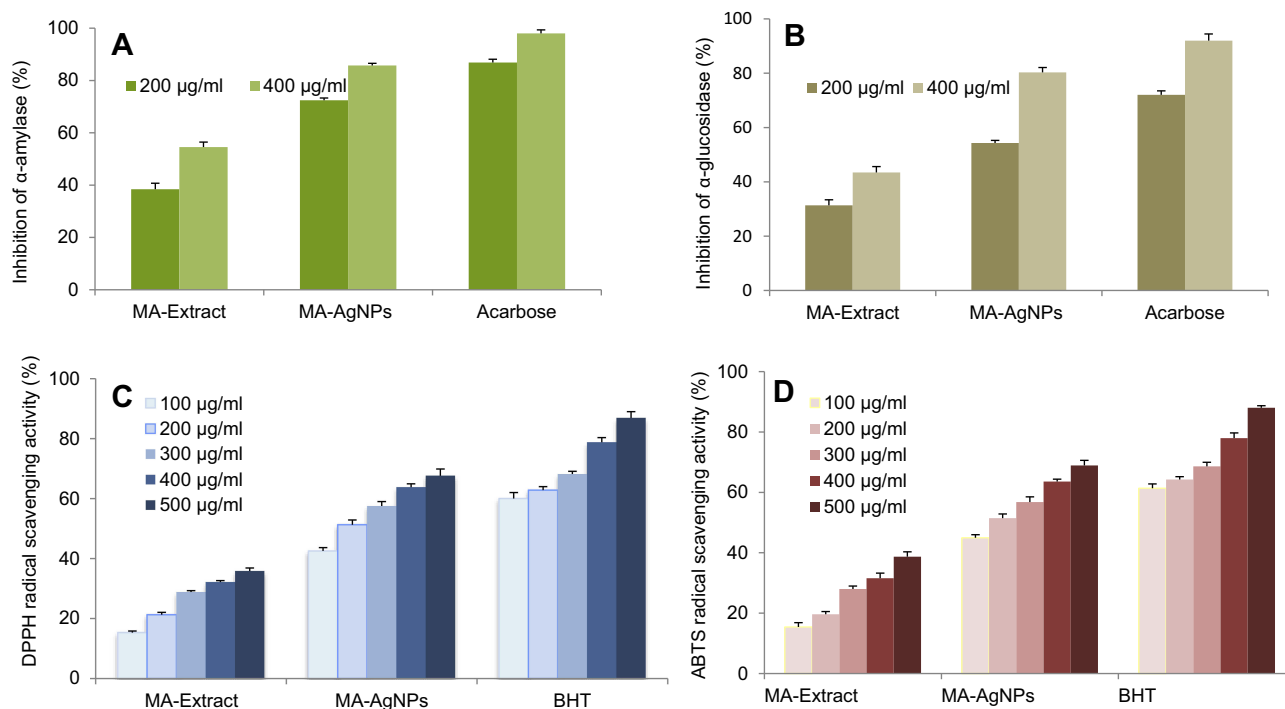
Figure 6 Antidiabetic and antioxidant potential of MA-extract and MA-AgNPs. **(A)** Percentage inhibition of α-amylase. **(B)** Percentage inhibition of α-glucosidase. **(C)** Percentage inhibition of DPPH radical. **(D)** Percentage inhibition of ABTS radical.

increase in the concentration of enzymes, a corresponding increase in the inhibitory activity was observed. MA-extract displayed 43.44±1.22% inhibition at maximum concentration (400 µg/mL), whereas MA-AgNPs exhibited nearly double the value at 80.33±1.94% (Figure 6B) for α-glucosidases inhibition. Interestingly, the MA-AgNPs had less α-glucosidase inhibition activity at lower concentration (54.32±0.93% at 200 µg/mL) which implies that the amount of MA-AgNPs can be easily reduced to control blood sugar level. The result confirmed that α-glucosidase inhibition effect was found to be more in MA-AgNPs than MA-extract. Similar to α-amylase, α-glucosidase also revealed a dose-dependent pattern. Effect of AgNO₃ on α-amylase inhibition (5.14±0.14%) and α-glucosidases enzyme inhibition (7.17±0.10%) was negligible.

Antioxidant Activity

Antioxidant activity of AgNO₃, MA-extract, and MA-AgNPs was examined by DPPH (Figure 6C) and ABTS (Figure 6D) radical scavenging assays in a dose-dependent manner. At the lowest concentration (100 µg/mL) MA-extract demonstrated 15.33±1.09% activity for DPPH radical scavenging and 15.40±1.01% for ABTS radical scavenging. These values increased to 35.86±2.18% and 38.68±1.66% for DPPH and ABTS radical scavenging respectively when concentration was increased to 500 µg/mL. Lowest concentration (100 µg/mL) for MA-AgNPs was at 42.54±1.98% for DPPH radical scavenging and 44.98±1.42% for ABTS radical scavenging respectively. The values increased to 67.66±2.05% and 68.94±0.67% for DPPH and ABTS radical scavenging when concentration was increased to 500 µg/mL. These results confirmed that, compared to MA-extract, MA-AgNPs exhibited higher scavenging activity. AgNO₃ exhibited negligible amount of antioxidant property against DPPH (7.08±0.01%) and ABTS (8.4±0.8%) radical scavenging assays.
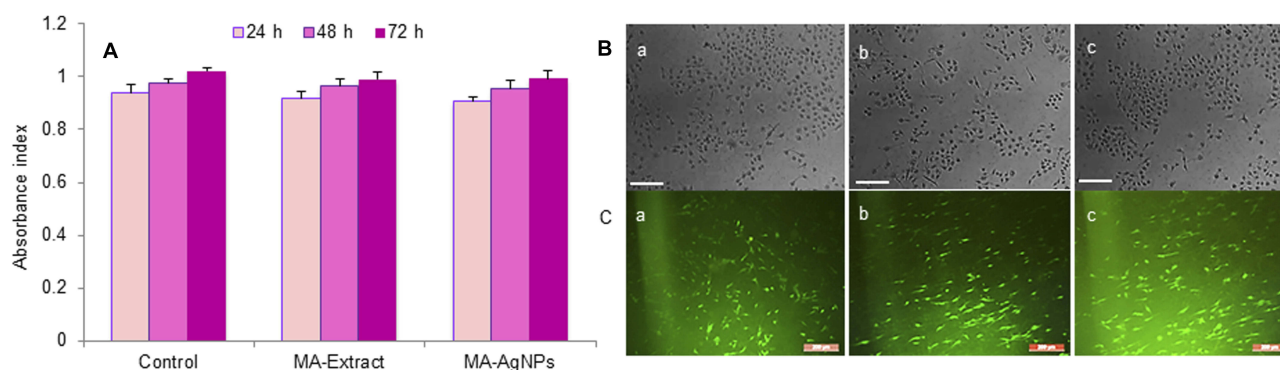
Cytotoxicity

MA-AgNPs demonstrated biological activity over a wide range of concentrations. To determine the safety of these MA-AgNPs for human use, MTS assay was performed at three different time points (24 h, 48 h, and 72 h) and cytotoxic effect of MA-AgNPs on CCL-13 cell line was analyzed at 1000 µg/mL as shown in Figure 7A. AgNPs treated cells had a viability of 92-94% for up to 72 h. In CCL-13 cell lines, we observed insignificant cytotoxic effect in microgram levels of MA-AgNPs. Additionally, the optical microscopic image (Figure 7B) and CMFDA dye studies (Figure 7C) did not show any morphological difference in the cells treated with control (a), MA-extract (b) and MA-AgNPs (c) at 72 h. These results proved that green synthesized MA-AgNPs were not toxic to human cells in low concentrations.

Discussion

Inert, less toxic, stable nature of plant extracts coupled with simple and efficient manufacturing techniques; make them a viable choice over the physical and chemical methods in synthesis of nanoparticles.[28] Thus, traditional medicinal values of leaf extract of *Melia azedarach*, were utilized in the current study. The nanoparticles have smaller size and hence larger surface area to volume ratio in comparison with the bulk made up of larger molecules. This makes nanoparticles more chemically reactive. Our results confirmed successful conversion of inert or less active MA-extract to highly active MA-AgNPs via bio reduction; with enhanced biological properties.

Green synthesized MA-AgNPs were analyzed using UV-Visible spectroscopy to determine the optimal concentration of

Figure 7 Cytotoxic effect of AgNPs on chang liver cell lines **(A)** MTS assay. **(B)** Optical microscopic image. **(C)** CMFDA dye analysis of (a) control, (b) MA-extract, (c) MA-AgNPs at 10x magnifications (scale bar: 200 µm).

MA-extract, AgNO$_3$, pH of reaction mixture and the incubation time required to obtain good yield. Controlled biosynthesis led to specific particle morphology in terms of size, shape, and arrangement. The optimization process plays an important role in increasing the NPs yield, morphology, aggregation, and stability.[29,30] By varying the ratio of AgNO$_3$ to MA-extract, we were able to synthesize MA-AgNPs less than 20 nm in size. Addition of 5 mL of MA-extract to 45 mL of 1 mM AgNO$_3$ (ratio 1:9) gave the best yield of MA-AgNPs. Any change in this ratio resulted in reduced synthesis of MA-AgNPs, due to unavailability of biomolecules. The intensity of color change of the reaction mixture (AgNO$_3$ + MA-extract) was directly proportional to the time of incubation. Upon addition of MA-extract to the AgNO$_3$, a pale yellow color was observed which darkened with time. Maximum yield was obtained at 18 h when the color of reaction mixture had turned dark brown. Formation of NPs is identified visually by the color change, which is due to the surface plasma resonance, ie, with the decrease in the size of particles there is an increase in the excitation of the outer surface of electrons.[31] In addition to the color change, synthesis of MA-AgNPs was also confirmed by absorption pattern in UV-Vis spectroscopy with presence of maximum absorption peak for silver in the range 400–450 nm and highest surface plasma resonance at 420 nm. The size of particles remained small while the yield of MA-AgNPs increased up to pH 7. This could be due to the binding of reactive functional groups with silver ion. After pH 10, particles increased in size which led to the shift of absorption maximum to longer wavelengths as less energy is required for excitation of electrons. With further increase in the pH, particles became unstable and agglomerated. As the phytochemicals present in the leaf extracts changed with the change in pH; the shape, size and stability of MA-AgNPs were also affected. This affected the capping and stabilizing ability. As reported in literature, pH 7 was found to be ideal for synthesis for AgNPs.[30] In our experiments, synthesis of MA-AgNPs was carried out at RT thus saving energy. AgNP formation has been reported at ambient[13] as well as at high temperatures.[12] As most of our experiments on MA-AgNPs activities were carried out within a week of their synthesis, we evaluated the stability up to nine days. The MA-AgNPs were found to be stable during this test period as determined by the UV-Vis spectroscopy where no change was observed in the maximum absorption peak (at 420 nm). Phytochemicals present in plants reduce the metal ions. Flavonoids, terpenoids, sucrose, and amides are some of the phytochemicals associated with bio-reduction of nanoparticles.[32]

Structural information of the formed MA-AgNPs was obtained by SEM, EDX, TEM, XRD, and FTIR analysis. MA-AgNPs were mostly spherical and some cuboidal in shape in SEM images. TEM images confirmed well dispersed MA-AgNPs in a size range of 14–20 nm. Different functional groups of phytochemicals present in the NPs contributed to different shapes, which help in reducing and stabilizing the NPs during formation.[33] FTIR spectral data indicated the reducing role of bioactive molecules present in MA-extract. Presence of terpenoids, flavonoids, and phenolic compounds was demonstrated by stretching vibration band at 2349 cm^{-1} (O=C=O) in *Prosopis juliflora* and 1457 cm^{-1} (CH) and 1640 cm^{-1} (C=C) in Propolis.[34,35] Our FTIR data showed, the predominant peak of OH and C=C on the surface of the MA-AgNPs and implied presence of polyphenols. Preliminary phytochemical analysis also indicated the presence of phenolic compounds, flavonoids, and terpenoids in the MA-extract.

Biomedical applications of AgNPs synthesized from plant extracts have been reported.[29,36] Here, MA-AgNPs showed enhanced antibacterial potency against *B. cereus* and *E. coli*, even at low concentration in comparison with the corresponding leaf extract. This difference in antibacterial activity was due to smaller particle size in nanomaterial formation which resulted in more surface area for the extract molecules to adhere. Smaller size of MA-AgNPs also helped in easy penetration into the bacterial cell and exerted bactericidal effect. Increased cell length and reduced cell width were observed in cultures treated with MA-AgNPs. Smaller sizes (<50nm) of the NPs have been reported to play a major role in the interaction and infiltration into the bacterial cells exhibiting greater antibacterial property as compared to larger ones.[37] Biosynthesis of nanoparticles capped with phytochemicals such as phenols, flavonoids, tannins and quinones has been reported to enhance bactericidal effect.[3] This aspect is particularly significant to achieve beneficial outcomes for antibacterial resistance along with low toxicity to the human body.[13] Various mechanisms for antibacterial property of NPs have been proposed. The NPs permeate through the bacterial cell wall and interact with cellular contents to disrupt thus resulting in total cellular destruction leading to cell apoptosis. Formation of reactive oxygen species results in the destruction of cell wall components such as deoxy ribonucleic acid, lipids and proteins; once the cell wall ruptures the cytoplasmic fluids flow out.[38] Electrostatic interaction between opposite charges can be the mechanism for antibacterial activity of AgNPs. As evaluated from their isoelectric point,[39] the NPs have a net positive charge and bacterial cell walls have a net negative charge. The interaction between AgNPs and the cell

membrane components breaks cell walls and destroys the cells. The antibacterial effect of AgNPs is thus attributed to small size, large surface area, cytoplasmic fluids leakage from the bacterial cell membrane, cell death, and lack of cell division. It was observed that though the growth of both *B. cereus* and *E. coli* was inhibited, a larger ZOI was seen in *E. coli* as compared to *B. cereus* upon treatment with AgNPs. This variation in the ZOI is attributed to their cell wall composition. Gram negative bacteria such as *E. coli*, have a cell wall structure comprising two layers of lipid membrane flanking on either side of a thin layer of peptidoglycan in-between. On the other hand, Gram positive bacteria, such as *B. cereus* have a thicker peptidoglycan layer in the periplasmic space of the cell membrane. The AgNPs are thus able to penetrate more easily through the cell wall of *E. coli* than *B. cereus* and disrupt the cellular function of the bacteria.[8]

The antibacterial effect of MA-AgNPs against both positive and negative gram strains proved the potential in future application as broad-spectrum antibiotics in bandages, dressings or gels. Bacterial biofilms provide a barrier for resistance against antibiotics and microorganisms thrive under this protection. AgNPs are capable of not only penetrating into bacterial cell wall but also disrupting the biofilm barrier.[40] Larger surface area to mass ratio of AgNPs is responsible for this phenomenon. With the future prospects of use in formation of wound dressing, the wound healing potential was assessed by cell scratch assay. We observed that MA-AgNPs accelerated the migration of fibroblasts. This indicated potential aid in wound healing. Similar observations have been reported in studies on mouse fibroblast cells.[23] Application of plant derived AgNPs in wound healing and their mechanism of action has been demonstrated in in vivo studies in rabbit.[41,42] Different types of NPs induce different cellular responses based on their physical and chemical properties such as size, shape, charge, and surface stimulation.[23] In our study, the green synthesized AgNPs showed negligible toxic effect.

The carbohydrate metabolism, particularly conversion of oligosaccharides and disaccharides into monosaccharides, is facilitated by the pancreatic α-amylase and intestinal α-glucosidase enzymes.[43] Non-insulin diabetes can be treated by limiting the activity of these two enzymes as this slows the discharge of glucose into the bloodstream.[44,45] The lowering of hyperglycemia prevents the associated macrovascular and microvascular conditions.[46] In our study, inhibitory action at two different concentrations (200 μg/mL and 400 μg/mL) of the AgNO₃, MA-extract and MA-AgNPs against the α-amylase and α-glucosidase enzymes was investigated. The results proved that compared to MA-extract, MA-AgNPs have

significant inhibitory activity toward the enzymes while the AgNO₃ alone had negligible enzyme inhibitory activity. α-amylase, α-glucosidase inhibitors like acarbose have a pseudosugar ring with a glycosidic nitrogen linkage that mimics the transition state for enzymatic cleavage of glycosidic bonds thereby inhibiting the action of amylase enzyme.[47] Higher activity of biosynthesized AgNPs in comparison to its leaf extracts has been reported in *Ficus glomerata*.[48] The AgNPs have shown higher antidiabetic activity than using just the extracts from other plants namely *Murraya koeniggii, Bougainvillea spectabilis, Ocimum tenuiflorum, Syzygium cumini*, and *Azadirachta indica*.[49] Further, MA-AgNPs had higher activity at much lower concentrations than AgNPs reported from plants like *Sphaeranthus amaranthoides* and *Halymenia poryphyroides*.[50]

Oxidative stress is linked with pathobiology of several diseases including aging, diabetes, cardiovascular disease, chronic inflammation, atherosclerosis, cancer, and other degenerative diseases. Antioxidant molecules quench the free radical reaction against oxidative stress and thus inhibit or delay oxidative damage to the biomolecules (lipids, proteins, DNA).[51,52] In our study, antioxidant activity at five different concentrations of MA-extract, AgNPs and BHT (as the reference standard) against DPPH and ABTS radical was analyzed. DPPH and ABTS radicals deactivated either by reduction, via e-transference or by free radical quenching via H⁺ transmission. Our DPPH and ABTS assays confirmed the synthesized MA-AgNPs had significantly higher (p≤0.01) scavenging activity compared to the MA-extract. The potential antioxidant ability of AgNP is due to the presence of phenolics, terpenoids, and flavonoids present in plants which allow AgNPs to act as singlet oxygen quenchers, hydrogen donors, and reducing agents.[53] The potential DPPH and ABTS free radical scavenging activities of AgNPs reported earlier have supported results from our study.[54]

Possession of bactericidal, wound healing, antidiabetic and antioxidant properties makes MA derived AgNPs suitable for manufacturing of bactericidal products, to aid in diabetic wound healing and in development of health supplements.

Conclusion

Green synthesis of stable, well distributed, crystalline and spherical MA-AgNPs (size 14–20 nm) from bio-reduction of AgNO₃ by MA-extract was confirmed by UV-Vis spectroscopy, SEM-EDX, TEM, XRD and FTIR analysis. MA-AgNPs showed significantly higher bioactivities in comparison with the MA-extract. The excellent antibacterial

activities of MA-AgNPs against both gram negative and gram positive bacteria make them suitable candidates for development of antibiotics against species resistant to conventional antibiotics. HDFa cell scratch assay proved MA-AgNPs have higher potential in wound healing than MA-extract. α-amylase and α-glucosidase inhibition proved that the MA-AgNPs have potential antidiabetic activity and DPPH and ABST assays confirmed increased antioxidant activity of MA-AgNPs compared to the MA-extract. Cytotoxic effect of MA-AgNPs on CCL-13 was negligible, this indicates its potential safe use for human applications. It was concluded that our green synthesis method is a simple, rapid, stable, and sustainable way of producing MA-AgNPs. This can be easily scaled-up for large scale production of nanoparticles using the waste product (leaves) from commercial timber plantations of *Melia azedarach*. This research can be further exploited for broad-spectrum bactericidal, wound healing, antidiabetic, and antioxidant applications.

Acknowledgments

Disclosure

The authors report no conflicts of interest in this work.

References

1. Mukherjee PK, Maiti K, Mukherjee K, Houghton PJ. Leads from Indian medicinal plants with hypoglycemic potentials. *J Ethnopharmacol*. 2006;106(1):1–28. doi:10.1016/j.jep.2006.03.021

2. Yuan H, Ma Q, Ye L, Piao G. The traditional medicine and modern medicine from natural products. *Molecules*. 2016;21(5):559. doi:10.3390/molecules21050559

3. Khatoon N, Mazumder JA, Sardar M. Biotechnological applications of green synthesized silver nanoparticles. *J Nanosci Curr Res*. 2017;2(1):107. doi:10.4172/2572-0813.1000107

4. Mohammadlou M, Maghsoudi H, Jafarizadeh-Malmiri H. A review on green silver nanoparticles based on plants: synthesis, potential applications and eco-friendly approach. *Int Food Res J*. 2016;23(2):446–463.

5. Ocsoy I, Tasdemir D, Mazicioglu S, Tan W. Nanotechnology in plants. *Adv Biochem Eng Biotechnol*. 2018;164:263–275. doi:10.1007/10_2017_53

6. Thakkar KN, Mhatre SS, Parikh RY. Biological synthesis of metallic nanoparticles. *Nanomedicine*. 2010;6(2):257–262. doi:10.1016/j.nano.2009.07.002

7. Makarov VV, Love AJ, Sinitsyna OV, et al. "Green" nanotechnologies: synthesis of metal nanoparticles using plants. *Acta Naturae*. 2014;6(1):35–44. doi:10.32607/20758251-2014-6-1-35-44

8. Ramanathan S, Gopinath SCB, Anbu P, et al. Eco-friendly synthesis of Solanum trilobatum extract-capped silver nanoparticles is compatible with good antimicrobial activities. *J Mol Struct*. 2018;1160:80–91. doi:10.1016/j.molstruc.2018.01.056

9. Monopoli MP, Aberg C, Salvati A, Dawson KA. Biomolecular coronas provide the biological identity of nanosized materials. *Nat Nanotechnol*. 2012;7(12):779–786. doi:10.1038/nnano.2012.207

10. Jiang W, Rutherford D, Vuong T, Liu H. Nanomaterials for treating cardiovascular diseases: a review. *Bioact Mater*. 2017;2(4):185–198. doi:10.1016/j.bioactmat.2017.11.002

11. Ge L, Li Q, Wang M, Ouyang J, Li X, Xing MM. Nanosilver particles in medical applications: synthesis, performance and toxicity. *Int J Nanomedicine*. 2014;9:2399–2407. doi:10.2147/IJN.S55015

12. Wang C, Mathiyalagan R, Kim YJ, et al. Rapid green synthesis of silver and gold nanoparticles using Dendropanax morbifera leaf extract and their anticancer activities. *Int J Nanomedicine*. 2016;11:3691–3701. doi:10.2147/IJN.S97181

13. Salehi S, Shandiz SA, Ghanbar F, et al. Photosynthesis of silver nanoparticles using Artemisia marschalliana Sprengel aerial part extract and assessment of their antioxidant, anticancer and antibacterial properties. *Int J Nanomedicine*. 2016;11:1835–1846. doi:10.2147/IJN.S99882

14. Orwa C, Mutua A, Kindt R, Jamnadass R, Simons A. *Agroforestree Database: A Tree Reference and Selection Guide Version 4.0*. Kenya: World Agroforestry Centre; 2009.

15. Mehmood A, Murtaza G, Bhatti TM, Kausar R. Phyto-mediated synthesis of silver nanoparticles from Melia azedarach L. leaf extract: characterization and antibacterial activity. *Arab J Chem*. 2017;10(2): S3048–S3053. doi:10.1016/j.arbjc.2013.11.046

16. Ramanibai R, Velayutham K. Bioactive compound synthesis of Ag nanoparticles from leaves of Melia azedarach and its control of mosquito larva. *Res Vet Sci*. 2015;98:82–88. doi:10.1016/j.rvsc.2014.11.009

17. Pani A, Lee JH, Yun SI. Autoclave mediated one-pot-one-minute synthesis of AgNPs and Au-Ag nanocomposite from Melia azedarach bark extract with antimicrobial activity against food pathogens. *Chem Cent J*. 2016;10:15. doi:10.1186/s13065-016-0157-0

18. Chandirika JU, Selvi ST, Annadurai G. Synthesis and characterization of silver nanoparticle using Melia azedarach for vegetable coating and antibacterial activity. *J Innovations Pharma Biol Sci*. 2018;5:38–42.

19. Sukirtha R, Priyanka KM, Antony JJ, et al. Cytotoxic effect of green synthesized silver nanoparticles using Melia azedarach against in vitro HeLa cell lines and lymphoma mice model. *Process Biochem*. 2012;47(2):273–279. doi:10.1016/j.procbio.2011.11.003

20. Ahmad N, Sharma S, Alam MK, et al. Rapid synthesis of silver nanoparticles using dried medicinal plant of basil. *Colloids Surf B Biointerfaces*. 2010;81(1):81–86. doi:10.1016/j.colsurfb.2010.06.029

21. Lee YJ, Song K, Cha SH, Cho S, Kim YS, Park Y. Sesquiterpenoids from Tussilago farfara flower bud extract for the eco-friendly synthesis of silver and gold nanoparticles possessing antibacterial and anticancer activities. *Nanomaterials*. 2019;9(6):819. doi:10.3390/nano9060819

22. Bauer AW, Kirby WM, Sherris JC, Turck M. Antibiotic susceptibility testing by a standardized single disk method. *Am J Clin Pathol*. 1966;45(4):493–496. doi:10.1093/ajcp/45.4_ts.493

23. Ahn EY, Jin H, Park Y. Assessing the antioxidant, cytotoxic, apoptotic and wound healing properties of silver nanoparticles green synthesized by plant extracts. *Mater Sci Eng C Mater Biol Appl*. 2019;101:204–216. doi:10.1016/j.msec.2019.03.095

24. Kazeem MI, Adomson JO, Ogunwandle IA. Mode of inhibition of α-amylase and α-glucosidase by aqueous extract of Moringa lucida leaf. *Biomed Res Int*. 2013;3:1–7. doi:10.1155/2013/527570

25. Yokozawa T, Chen CP, Dong E, Tanaka T, Nonaka GI, Nishioka I. Study on the inhibitory effect of tannins and flavonoids against 1,1-diphenyl-2 picrylhydrazyl radical. *Biochem Pharmacol*. 1998;56(2):213–222. doi:10.1016/s0006-2952(98)00128-2

26. Miller NJ, Rice-Evans CA. Factors influencing the antioxidant activity determined by ABTS•+ radical cation assay. *Free Radic Res*. 1997;26(3):195–199. doi:10.3109/10715769709097799

27. Gandhimathi C, Venugopal JR, Bhaarathy V, Ramakrishna S, Kumar SD. Biocomposite nanofibrous strategies for the controlled release of biomolecules for skin tissue regeneration. *Int J Nanomedicine*. 2014;9(1):4709–4722. doi:10.2147/IJN.S65335

28. Roy A, Bulut O, Some S, Mandal AK, Yilmaz MD. Green synthesis of silver nanoparticles: biomolecule-nanoparticle organizations targeting antimicrobial activity. *RSC Adv*. 2019;9:2673–2702. doi:10.1039/C8RA08982E

29. Veerasamy R, Xin TZ, Gunasagaran S, et al. Biosynthesis of silver nanoparticles using mangosteen leaf extract and evaluation of their antimicrobial activities. *J Saudi Chem Soc*. 2011;15(2):113–120. doi:10.1016/j.jscs.2010.06.004

30. Khalil MM, Ismail EH, El-Magdoub F. Biosynthesis of Au nanoparticles using olive leaf extract: 1st nano updates. *Arab J Chem*. 2012;5 (4):431–437. doi:10.1016/j.arabjc.2010.11.011

31. Wiley BJ, Im SH, Li ZY, McLellan J, Siekkinen A, Xia Y. Maneuvering the surface plasmon resonance of silver nanostructures through shape-controlled synthesis. *J Phys Chem B*. 2006;110 (32):15666–15675. doi:10.1021/jp0608628

32. Singh J, Dutta T, Kim KH, Rawat M, Samddar P, Kumar P. 'Green' synthesis of metals and their oxide nanoparticles: application for environmental remediation. *J Nanobiotechnology*. 2018;16(1):84. doi:10.1186/s12951-018-0408-4

33. Bootz A, Vogel V, Schubert D, Kreuter J. Comparison of scanning electron microscopy, dynamic light scattering and analytical ultracentrifugation for the sizing of poly(butyl cyanoacrylate) nanoparticles. *Eur J Pharm Biopharm*. 2004;57(2):369–375. doi:10.1016/S0939-6411(03)00193-0

34. Malik SK, Ahmed M, Khan F. Identification of novel anticancer terpenoids from Prosopis juliflora (Sw) DC (Leguminosae) pods. *Trop J Pharm Res*. 2018;17(4):661–668. doi:10.4314/tjpr.v17i4.14

35. Oliveira RN, Mancini MC, Oliveira FCS, et al. FTIR analysis and quantification of phenol and flavonoids of five commercially available plant extracts used in wound healing. *Revistamateria*. 2016;11743:767–779. doi:10.1590/S1517-707620160003.0072

36. Burdusel AC, Gherasim O, Grumezescu AM, Mogoanta L, Anton F, Andronescu E. Biomedical application of silver nanoparticles: an upto-date overview. *Nanomaterials*. 2018;8(9):681. doi:10.3390/nano8090681

37. Gurunathan S, Han JW, Kwon DN, Kim JH. Enhanced antibacterial and anti-biofilm activities of silver nanoparticles against gram-negative and gram-positive bacteria. *Nanoscale Res Lett*. 2014;9(1):373. doi:10.1186/1556-276X-9-373

38. Kumar RS, Maddirevula S, Easwaran M, Dananjaya SHS, Kim MD. Antibacterial activity of novel Cu_2ZnSnS_4 nanoparticles against pathogenic strains. *RSC Adv*. 2015;5(129):106400–106405. doi:10.1039/C5RA15027B

39. Lokhande AC, Shelke A, Babar PT, Lokhandee CD, Kim JH. Novel antibacterial application of photovoltaic Cu_2SnS_3 (CTS) nanoparticles. *RSC Adv*. 2017;7:33737–33744. doi:10.1039/C7RA05194H

40. Wang L, Hu C, Shao L. The antimicrobial activity of nanoparticles: present situation and prospects for the future. *Int J Nanomedicine*. 2017;12:1227–1249. doi:10.2147/IJN.S121956

41. Haseeb MT, Hussain MA, Abbas K, et al. Linseed hydrogel-mediated green synthesis of silver nanoparticles for antimicrobial and wound-dressing applications. *Intl J Nanomed*. 2017;12:2845–2855. doi:10.2147/IJN.S133971

42. Muhammad G, Hussain MA, Amin M, et al. Glucuronoxylan-mediated silver nanoparticles: green synthesis, antimicrobial and wound healing applications. *RSC Adv*. 2017;7:42900–42908. doi:10.1039/c7ra07555c

43. Inzucchi SE. Oral antihyperglycemic therapy for type 2 diabetes. *JAMA*. 2002;287(3):360–372. doi:10.1001/jama.287.3.360

44. Sales PM, Souza PM, Simeoni LA, Magalhães PO, Silveira D. α-Amylase inhibitors: a review of raw material and isolated compounds from plant source. *J Pharm Sci*. 2012;15(1):141–183. doi:10.18433/J35S3K

45. Podsedek A, Majewska I, Redzynia M, Sosnowska D, Koziołkiewicz M. In vitro inhibitory effect on digestive enzymes and antioxidant potential of commonly consumed fruits. *J Agric Food Chem*. 2014;62 (20):4610–4617. doi:10.1021/jf5008264

46. Patel DK, Kumar R, Laloo D, Hemalatha S. Diabetes mellitus: an overview on its pharmacological aspects and reported medicinal plants having antidiabetic activity. *Asian Pac J Trop Biomed*. 2012;2(5):411–420. doi:10.1016/S2221-1691(12)60067-7

47. Robyt JF. Inhibition, activation and stabilization of α-amylase family enzymes. *Biologia Bratislava*. 2005;60(16):17–26.

48. Das MP, Devi PV, Yasmine Y. Assessment of in vitro anti-diabetic activity of Ficus glomerata. *Der Pharma Lett*. 2016;8:267–272.

49. Bhat M, Zinjarde SS, Bhargava SY, Kumar AR, Joshi BN. Antidiabetic Indian plants: a good source of potent amylase inhibitors. *Evid Based Complement Alternat Med*. 2011;810207. doi:10.1093/ecam/nen040

50. Anand K, Tiloke C, Naidoo P, Chuturgoon AA. Phytonanotherapy for management of diabetes using green synthesis nanoparticles. *J Photochem Photobiol B*. 2017;173:626–639. doi:10.1016/j.jphotobiol.2017.06.028

51. Yu BP. Cellular defenses against damage from reactive oxygen species. *Physiol Rev*. 1994;74(1):139–162. doi:10.1152/physrev.1994.74.1.139

52. Dehpour AA, Ebrahimzadeh MA, Fazel NS, Mohammed NS. Antioxidant activity of methanol extract of Ferula assafoetida and its essential oil composition. *Grasas Y Aceites*. 2009;60(4):405–412. doi:10.3989/gya.010109

53. Chang ST, Wu JH, Wang SY, Kang PL, Yang NS, Shuyur LF. Antioxidant activity of extracts from Acacia confusa bark and heartwood. *J Agric Food Chem*. 2001;49(7):3420–3424. doi:10.1021/jf0100907

54. Seralathan J, Stevenson P, Subramaniam S, et al. Spectroscopy investigation on chemo-catalytic, free radical scavenging and bactericidal properties of biogenic silver nanoparticles synthesized using Salicornia brachiata aqueous extract. *Spectrochim Acta a Mol Biomol Spectrosc*. 2014;118:349–355. doi:10.1016/j.saa.2013.08.114